

Delamination buckling of FRP layer in laminated wood beams

Youngchan Kim,^a Julio F. Davalos^{b*} & Ever J. Barbero^c

^aTechnology Research Institute, DAELIM Industrial Co., P.O. Box 1117, Seoul, Korea

^bDepartment of Civil and Environmental Engineering, West Virginia University, Morgantown, WV 26506-6103, USA

^cDepartment of Mechanical and Aerospace Engineering, West Virginia University, Morgantown, WV 26506-6103, USA

An analytical solution for predicting delamination buckling and growth of a thin fiber reinforced-plastic (FRP) layer in laminated wood beams under bending is presented. Based on a strength-of-materials approach, displacement functions for a delaminated beam under four-point bending are derived. Using force and displacement compatibility conditions, an explicit form relating the applied transverse load with the delamination buckling load is established. An explicit form of the strain-energy release rate is presented to study the delamination growth in beams under bending. The analytical solution is evaluated using experimental data for glued-laminated timber (glulam) beams reinforced with a thin fiber-reinforced plastic composite on the compression face. The delamination growth in bending is shown to behave differently to that of the in-plane loading case.
 © 1997 Elsevier Science Ltd.

NOTATION

The notation used in this paper is listed below.

A_i	Axial stiffness of segment i
b	Beam width
D_i	Bending stiffness of segment i
G	Strain-energy release rate
G_{ic}	Critical strain-energy release rate
h	Thickness of delaminated layer
L	Beam span length
L_d	Delamination length
L_o	Loading span length
M_i	Moment acting on segment i
P	Internal axial force acting on segment 3
Q	Applied transverse load
t	Beam thickness
w_i	Transverse deflection for segment i
w_{2max}	Displacement at mid-span
ϵ_3	Strain of a delaminated layer
ϵ_3^{exp}	Experimental ϵ_3
δ	Prescribed displacement at the end of a delaminated layer

Δ	Displacement at the loading point
θ	Prescribed rotation at the end of a delaminated sublaminde

INTRODUCTION

Delamination in composite laminates causes separation of an adjoining layer from the main laminate structure. Delamination growth may significantly influence the strength, stiffness and stability of a laminate. The initiation of delamination results from many sources, such as manufacturing defects, deterioration of bonding materials, or local impact damage. The delamination behavior in laminated structures has received the attention of several investigators.

One of the first analytical delamination models was developed by Chai [1]. He characterized the delamination in homogeneous, isotropic plates using a thin-film model, and extended this approach to a general bending case which included the bending of a thick base laminate. Including bending-extension coup-

*Author to whom correspondence should be addressed.

ling, Yin [2] derived general formulae for thin-film strips and mid-plane symmetric delaminations in composite laminates. Kardomateas and Schmueser [3] analyzed the deformation of delaminated composite under axial loading with a one-dimensional beam-plate model including transverse shear effects. Chen [4] developed a shear deformation theory for compressive delamination buckling and growth with a variational energy principle.

The nonlinear behavior of a composite delaminated beam under axial loading was analyzed by Sheinman and Soffer [5]. Tracy and Pardo [6] studied the effect of delamination on the flexural stiffness of laminated beams, but their analytical solution did not include bending-extension coupling or delamination buckling. They tested specimens manufactured with a delamination at the mid-plane, and they concluded that the delamination did not degrade much the stiffness of the laminates. However, as observed in glulam-FRP beam tests [7], if the delamination was placed near the top surface of a beam, delamination buckling is likely to occur. Consequently, the stiffness of the beam would be affected substantially.

Reddy *et al.* [8] developed a generalized laminate plate theory (GLPT), and used this theory to account for multiple delaminations between layers. The associated finite-element model was developed by Barbero [9] and Barbero and Reddy [10]. Based on GLPT, Lee *et al.* [11] developed a displacement-based, one-dimensional finite-element model to predict critical loads and corresponding buckling modes for a multiply delaminated composite with arbitrary boundary conditions. Sankar [12] developed an offset-node beam finite element to model delaminations in composite beams. The modeling of delaminations in a composite beam, however, was limited to the case of two sublaminates with the same thickness, one above and one below the delamination plane. The offset-node element was extended to the study of dynamic delamination propagation in composite beams [13]. Most of the existing studies focused on the response of a delaminated thin laminate (thin-film delamination) which does not affect the strength and stability of a thick-base laminate. Recently, Kutlu & Chang [14] investigated the compressive response of laminated composites with multiple delaminations, including the interaction between the delamination growth and the response of laminates.

In a hybrid system, such as glued-laminated timber beams (glulam) reinforced with fiber-reinforced plastic (FRP) strips, different materials are bonded with an adhesive and, therefore, loss of face-to-face local adhesion is the main cause of delamination at the interfaces of two distinct layers. Reinforcing glulam beams with FRP strips on the compression and/or tension side is an efficient way to increase the stiffness and strength of laminated wood beams and to decrease the depth of the member [7]. Usually, the thickness of a FRP strip is very small compared to that of a glulam beam. For beams reinforced with FRP on the compression face, the debonding and subsequent local buckling of the FRP layer can result in a premature failure of a glulam-FRP beam. To predict the ultimate strength of glulam-FRP beams reinforced on the compression face, it is necessary to investigate the delamination behavior of a thin compression layer in a delaminated beam under bending.

In this paper, an analytical model to predict delamination buckling of a FRP strip in a reinforced laminated beam under bending is presented. The investigation of the critical loads and delamination behavior are the major concerns of this study. In the analytical model an initial delamination length at the interface of the top layer and the base laminate is assumed. Beyond the delamination length, the rest of the top layer remains bonded to the compression face of a relatively thick laminate. The delaminated beam is subjected to four-point bending and the initial delamination is symmetric about the mid-span. The displacement, rotation and the axial force acting at the delaminated layer are computed, based on the assumed displacement functions which are derived using boundary conditions and compatibility conditions. Also, explicit expressions for critical buckling load and strain-energy release rate are provided. Using the test data of a full-size laminated beam, the displacement and critical loads predicted by this study are compared with experimental values. A parametric study is carried out to investigate the effect of laminate stiffness on the critical loads. The strain-energy release rate for various initial delamination lengths are computed to find out the trend of delamination growth in laminated beams under bending. Finally, findings of this study are summarized and recommendations for future research are suggested.

DISPLACEMENT FUNCTIONS

In this paper the entire beam is involved in the derivation of the analytical solution. Consider the beam shown in Fig. 1 subjected to four-point symmetric loading, where one half of the beam is modeled using a shear-release at mid-span. The beam is divided into three segments: segment 1 contains no delamination; segment 2 is the base laminate, or thicker lower portion of the delaminated region; and segment 3 is the thin upper lamina that has undergone delamination. The subscripts used in the derivation of the theory correspond to these three segments.

The coordinate system and beam parameters are shown in Fig. 2. To simplify the problem of interest, we assume that a single symmetric delamination is present at mid-span before loading. Also we assume that mode I (opening mode) fracture is the primary mechanism for delamination growth, because the delaminated segment is in the shear-free zone, and that the thickness of a delaminated lamina is small compared to that of the laminated beam. The displacement functions in all three segments are

derived next, and the notation used is given in Appendix B.

From the support to the loading point: segment 1 ($0 < x_1 < L/2 - L_o/2$)

As the bending moment varies linearly in this region, the displacement function can be assumed as

$$w_{1a}(x_1) = ax_1^3 + bx_1^2 + cx_1 + d \tag{1}$$

The boundary condition at the support and constitutive equation are

$$w_{1a}(0) = 0, M = -D_1 w''_{1a} = Qx_1 \tag{2}$$

Then, we have

$$w_{1a}(x_1) = -\frac{Q}{6D_1} x_1^3 + cx_1 \tag{3}$$

The coefficient c will be determined in Section 2.2 using compatibility conditions.

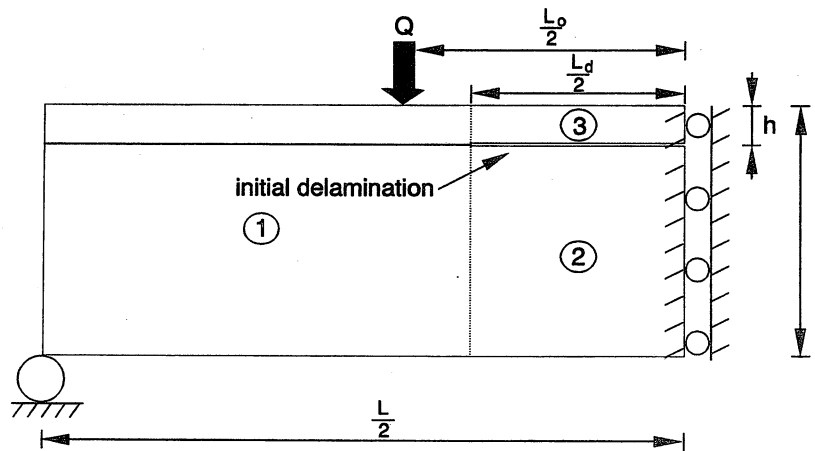


Fig. 1. Delaminated beam configuration.

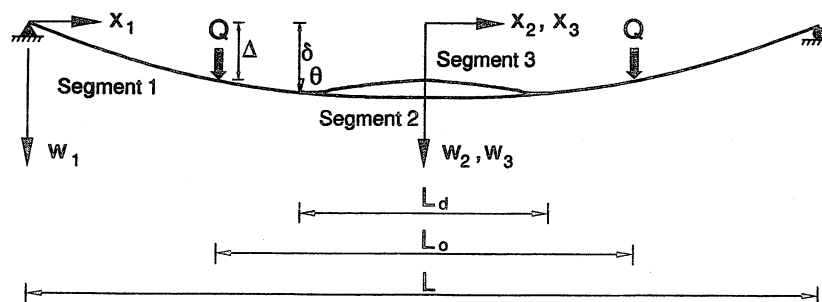


Fig. 2. Coordinate system.

From the loading point to the delamination tip:
segment 1 ($L/2 - L_o/2 < x_1 < L/2 - L_d/2$)

As the bending moment is constant in this region, the displacement function can be written as

$$w_{1b}(x_1) = ex_1^2 + fx_1 + g \quad (4)$$

The constitutive relation and the prescribed boundary conditions at the delamination tip are

$$w_{1a} = \left(\frac{L}{2} - \frac{L_d}{2} \right) = \delta, w'_{1b} \left(\frac{L}{2} - \frac{L_d}{2} \right) = \theta, \quad (5)$$

$$M = -D_1 w_{1b} = Q \left(\frac{L}{2} - \frac{L_d}{2} \right)$$

Then, we obtain

$$w_{1b}(x_1) = -\frac{Q(L-L_o)}{4D_1} x_1^2 + \left[\frac{Q(L-L_o)(L-L_d)}{4D_1} + \theta \right] x_1 + \delta - \frac{(L-L_d)}{2} \theta - \frac{Q(L-L_o)(L-L_d)^2}{16D_1} \quad (6)$$

The continuity condition of rotation at $x_1 = L/2 - L_o/2$ gives

$$c = \frac{Q(L-L_o)(L-2L_d+L_o)}{8D_1} + \theta \quad (7)$$

Then eqn (3) becomes

$$w_{1a}(x_1) = -\frac{Q}{6D_1} x_1^3 + \left[\frac{Q(L-L_o)(L-2L_d+L_o)}{8D_1} + \theta \right] x_1 \quad (8)$$

From the displacement continuity condition at $x_1 = L/2 - L_o/2$, we have

$$\theta = -\frac{Q(L-L_o)(L-L_d)}{8D_1} + \frac{Q(L-L_o)^3}{24D_1(L-L_d)} + \frac{2\delta}{(L-L_d)} \quad (9)$$

Delaminated region: segment 2 ($-L_d/2 < x_2 < 0$)

Assuming a constant bending moment in this region, the displacement function is given by

$$w_2(x_2) = hx_2^2 + ix_2 + j \quad (10)$$

Using the prescribed boundary conditions at the delamination tip, we have

$$w_2(x_2) = -\frac{\theta}{L_d} x_2^2 + \delta + \frac{\theta}{4} L_d \quad (11)$$

Delaminated region: segment 3 ($-L_d/2 < x_3 < 0$)

The post-buckling deflection shape of a beam-column is given as (Chen & Lui [15, p. 177])

$$w_3(x_3) = K_1 \sin(\alpha x_3) + K_2 \cos(\alpha x_3) + K_3 x_3 + K_4, \quad \alpha = \sqrt{\frac{P}{D_3}} \quad (12)$$

As the deformed shape is symmetric, we have $K_1 = K_3 = 0$. Using the compatibility of displacement δ and rotation θ at the interface between segments 1 and 3, eqn (12) becomes

$$w_3(x_3) = \frac{\cos(\alpha x_3) - \cos \beta}{\alpha \sin \beta} \theta + \delta \quad (13)$$

where

$$\beta = \frac{\alpha L_d}{2} \quad (14)$$

The displacement functions expressed in terms of beam parameters and the prescribed boundary conditions are used to compute strain energy and strain-energy release rate in a beam, as discussed next.

CRITICAL BUCKLING LOAD AND DELAMINATION GROWTH

Beam bending induces a strain distribution that is linear through the thickness of the beam. The linear strain distribution can be represented by resultant moments for segments 1 and 2 and resultant axial forces acting at segments 2 and 3, as shown in Fig. 3. From the moment equilibrium condition at the delamination tip, we can write

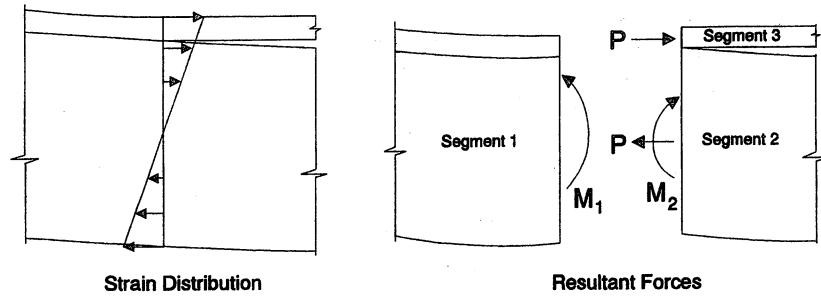


Fig. 3. Resultant forces at the delamination front.

$$M_1 = M_2 + \frac{Pt}{2} \quad (15)$$

The moment-curvature relations for M_1 and M_2 are

$$M_1 = -D_1 \frac{d^2 w_1}{dx^2} = \frac{Q(L-L_0)}{2} \quad (16)$$

$$M_2 = -D_2 \frac{d^2 w_2}{dx^2} = \frac{2D_2 \theta}{L_d}$$

Using eqns (15) and (16), θ can be expressed as

$$\theta = \frac{L_d}{4D_2} [Q(L-L_0) - Pt] \quad (17)$$

The compatibility condition of axial shortening of segments 2 and 3 is

$$\frac{P}{A_3} L_d = \frac{1}{2} \int_{-L_d/2}^{L_d/2} \left(\frac{dw_2}{dx_2} \right)^2 dx_2 + t\theta - \frac{P}{A_2} L_d \quad (18)$$

Then, we obtain

$$\theta = -\frac{3t}{L_d} + \sqrt{\frac{9t^2}{L_d^2} + 6 \left(\frac{1}{A_2} + \frac{1}{A_3} \right) P} \quad (19)$$

Equating eqns (17) and (19), the relation between P and Q is established as

$$Q = \frac{Pt}{(L-L_0)} - \frac{4D_2}{L_d(L-L_0)} \times \left[\frac{3t}{L_d} - \sqrt{\frac{9t^2}{L_d^2} + 6P \left(\frac{1}{A_2} + \frac{1}{A_3} \right)} \right] \quad (20)$$

Using the displacement functions given in eqns (6), (8), (11) and (13), the strain energy along the post-buckling path for each segment is com-

puted as follows. First, the bending energy for segment 1 is

$$U_1 = \frac{1}{2} D_1 \int_0^{L/2-L_d/2} \left(\frac{d^2 w_1}{dx^2} \right)^2 dx \quad (21)$$

$$= \frac{(L-L_0)^2 (L+2L_0-3L_d)}{48D_1} Q^2$$

The bending energy for segment 2 is

$$U_2 = \frac{1}{2} D_2 \int_0^{L_d/2} \left(\frac{d^2 w_2}{dx^2} \right)^2 dx \quad (22)$$

$$= \frac{L_d}{16D_2} [Q(L-L_0) - P_{cr}t]^2$$

and the membrane and bending energy for segment 3 is

$$U_3 = \frac{1}{2} \epsilon_{cr}^2 A_3 \frac{L_d}{2} + \frac{1}{2} D_3 \int_0^{L_d/2} \left(\frac{d^2 w_3}{dx^2} \right)^2 dx \quad (23)$$

$$= \frac{P_{cr}^2 L_d}{4A_3} + \frac{P_{cr} \theta^2}{8 \sin^2 \beta_{cr}} \left(L_d + \sin 2\beta_{cr} \sqrt{\frac{D_3}{P_{cr}}} \right)$$

As the thickness of a delaminated layer is very thin compared to that of the beam, Euler's column buckling formula for a fixed-fixed boundary condition can be used for P_{cr} [1]. Then, substituting P_{cr} from the Euler's column buckling formula into eqn (20), a critical transverse load Q_{cr} can be computed from eqn (20) which is valid up to the critical stage. An alternative procedure to find P_{cr} from the total potential energy is described in Appendix A. Note that in eqn (23), the load in the delaminated segment is assumed to remain constant and equal to P_{cr} . This is because of the virtually flat post-buckling path, similar to that of an Euler column.

The strain-energy release rate (G) is defined as

$$G = - \frac{\partial(U_1 + U_2 + U_3)}{\partial L_d} \quad (24)$$

and using eqns (16)–(23), the explicit expression of G per unit width is

$$G = \frac{(L - L_o)^2 Q^2}{8bD_1} - \frac{[Q(L - L_o) - P_{cr}t]^2}{8bD_2} - \frac{P_{cr}L_d^2[Q(L - L_o) - P_{cr}t]^2}{64bD_2^2 \sin \beta_{cr}} \times \left(2 - \sqrt{\frac{P_{cr}}{D_3} \frac{L_d}{\tan \beta_{cr}}} \right) \quad (25)$$

The accuracy of the model developed in this section is evaluated by correlating the analytical solutions with experimental results, as presented next.

NUMERICAL EXAMPLE

The test data for glulam beams reinforced with GFRP [7] are used to validate the analytical solution presented previously. The beam configuration and average layer material properties are shown in Fig. 4, and the beam parameters are listed in Table 1. The delaminated length (L_d), which is unknown at the time of the test, is a parameter needed to carry out the computations with the equations derived in Section 3. The delaminated length is estimated using lamination beam theory (LBT, Barbero [16])

and Euler's column buckling formula. The critical experimental load, $Q_{cr}^{exp} = 47.2$ kN, was recorded when buckling of the delaminated layer was observed during the experiment (see Fig. 5). Using LBT, the stress in the delaminated layer at buckling can be computed using the known critical load Q_{cr}^{exp} as follows

$$\sigma_{cr} = \frac{ME_i y_i}{D_1} = \frac{Q_{cr}^{exp}(L - L_o)E_i y_i}{2D_1} = 82 \text{ (kN/m}^2\text{)} \quad (26)$$

Assuming that the delaminated layer behaves like a fixed-fixed column, the approximate delamination length is computed from Euler's formula as

$$L_d = \sqrt{\frac{4D_3 \pi^2}{\sigma_{cr} h b}} = 0.16 \text{ (m)} \quad (27)$$

Using eqns (19) and (20), P and θ can be computed for a given Q . Then, the maximum mid-span deflection w_{2max} is given by eqn (11) as

$$w_{2max} = \delta + \frac{\theta}{4} L_d \quad (28)$$

The internal axial force P_{cr} in the delaminated lamina and the critical transverse load Q_{cr} are related by eqn (20). It is our interest to predict Q_{cr} which causes local buckling of a delaminated sublaminate. In Fig. 6, P_{cr} and Q_{cr} are plotted for various delamination lengths, where P_{cr} is computed from eqn (A5) and also Euler's formula, and Q_{cr} is obtained from eqn (20).

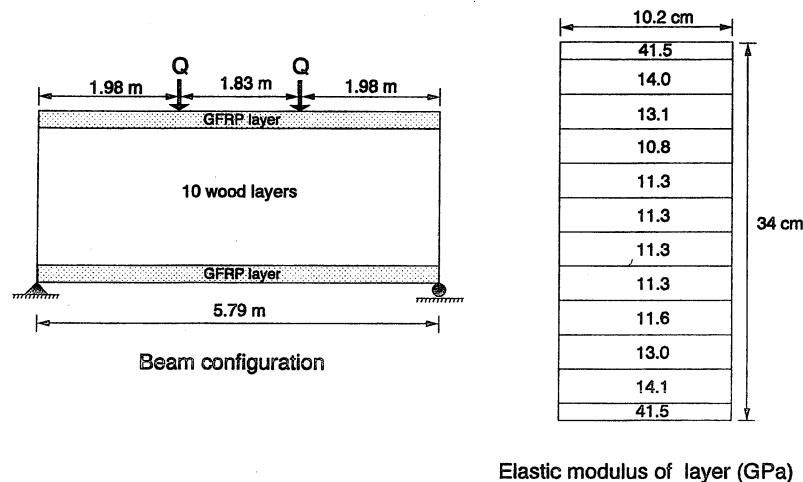


Fig. 4. Beam configuration and elastic modulus of each layer.

Table 1. Beam parameters

Length (m)	$L = 5.79, L_o = 1.83$
Axial stiffness (MN)	$A_2 = 428.8, A_3 = 20.1$
Bending stiffness (GN·m ²)	$D_1 = 7.96, D_2 = 7.03, D_3 = 5.87$
Thickness (cm)	$h = 0.48, t = 33.9$
Width (cm)	$b = 10.15$

Euler's formula and the results of eqn (A5) provide nearly identical values for P_{cr} . However, Euler's formula can not by itself provide any information on the magnitude of the transverse load (Q). Therefore, eqn (20) must be used. The experimental load–displacement path of the glulam–GFRP beam is given in Fig. 5, and the experimental values and analytical solutions are compared in Table 2. The mid-span maximum displacement relative to the point loads is underpredicted by 7.5%. One of the reasons for

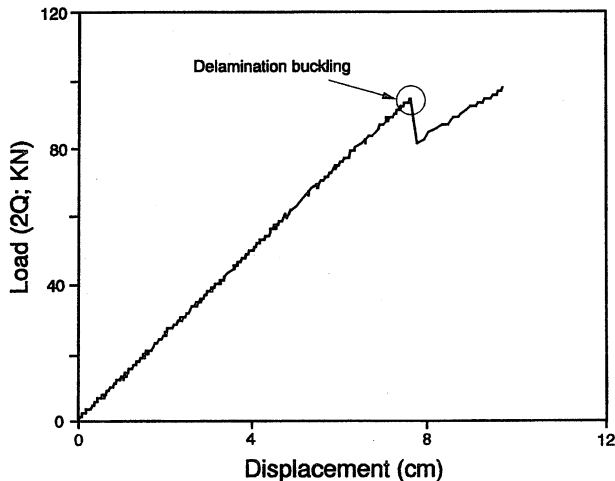


Fig. 5. Experimental load–displacement curve of the glulam–GFRP beam.

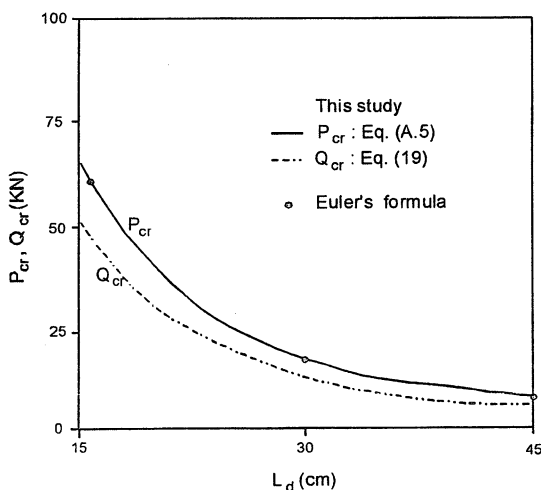


Fig. 6. Critical loads vs delamination length.

this difference is that the material properties of the wood layers vary along the length of the beam. Compared with test results, the critical load Q_{cr} predicted by this study is within 2.6% of the experimental value, and the predicted P_{cr} is within 1% of the experimental P_{cr} . The experimental P_{cr} is computed using the experimental strain at the top surface measured with strain gages.

To investigate the effect of the beam stiffness on Q_{cr} and P_{cr} the elastic moduli of the GFRP layer and wood layers are modified using multipliers as follows

$$E_{wood}^* = R_w E_{wood} \quad (29)$$

$$E_{composite}^* = R_c E_{composite}$$

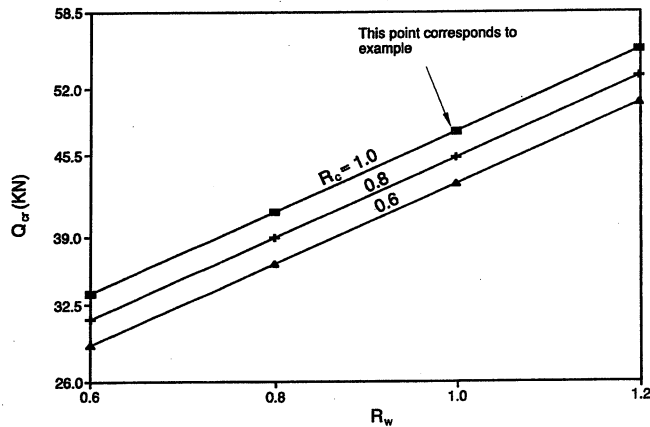
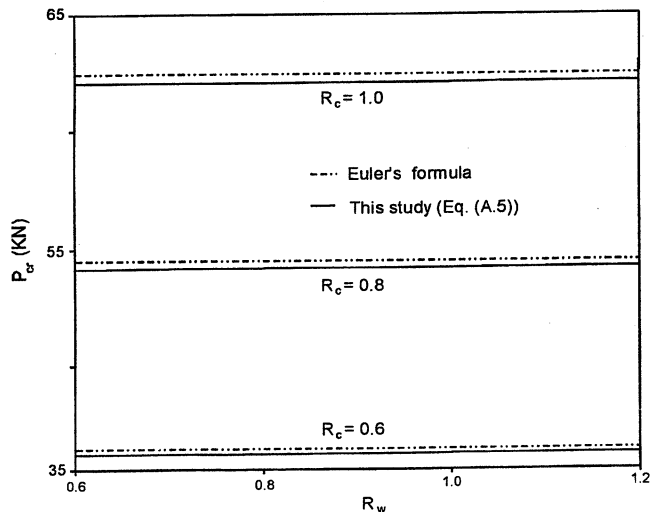
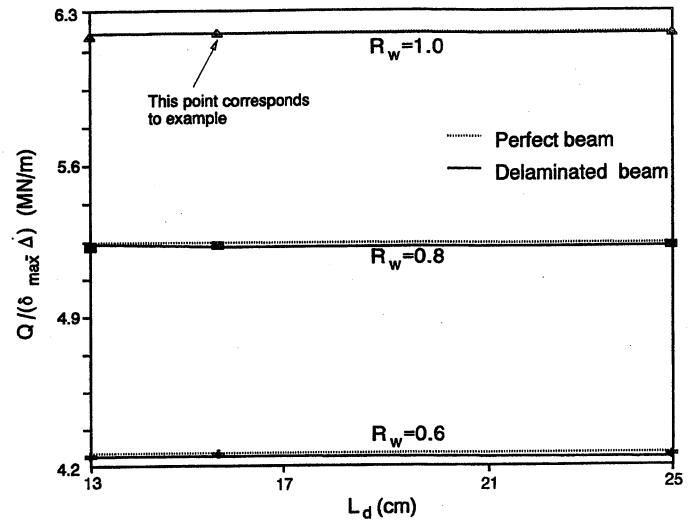
where $R_w = R_c = 1.0$ corresponds to the test beam parameters given in Table 1 and Fig. 4. As seen in Fig. 7, the response of Q_{cr} is linearly proportional to the value of the multipliers. As expected, increasing the elastic modulus of wood layers affect Q_{cr} more significantly than increasing the modulus of the top composite layer. The corresponding internal axial force P_{cr} is shown in Fig. 8. Unlike the curves for Q_{cr} , the value of P_{cr} is not affected by the bending stiffness of segment 2, and it depends only on the stiffness of segment 3. Therefore, only the material properties of the delaminated sublaminates affect the stress level in the delaminated layer. As in the case of Fig. 6, the value obtained by using eqn (A5) is almost identical to that computed with Euler's formula. To investigate the effect of delamination length on beam stiffness, the response of a delaminated beam is compared with that of a perfect beam, and the effect of wood properties is also explored for different values of R_w . As shown in Fig. 9, the degradation of the delaminated beam stiffness is not affected by the delamination length. However, the delamination length can significantly influence the state of stress in the delaminated sublaminates, and the ultimate strength and failure mode of the beam. After the buckling of a delaminated sublaminates occurs, it is of interest to investigate the growth of the delamination length; i.e. whether or not the delamination will grow or be arrested as function of the applied load. For this purpose, the strain-energy release rate given in eqn (25) is plotted for various initial delamination lengths in Fig. 10. To interpret the physical meaning of the curves, a critical strain-energy

Table 2. Comparison of critical load, force and displacement

$[w_{2\max} - \Delta]$ (mm)		Q_{cr} (kN)		P_{cr} (kN)		
Test	This study	Test	This study	Test ¹	Euler	eqn (A5)
8.37	7.74	47.2	48.5	61.9	61.5	61.4

$${}^1P_{cr} = (\epsilon_3^{\text{exp}})A_3 = (3.08 \times 10^{-3}) (20.1).$$

release rate (G_{IC}) is assumed as 87.6 N/m. This value of G_{IC} is representative of graphite-epoxy T300/976 (see [14]). When the transverse load reaches a critical value ($Q_{cr} = 48.5$ kN for the example considered in this study), the delamination becomes unstable, and it grows from the initial delamination length ($L_d = 0.16$ m) to a stable condition ($L_d = 0.3$ m). Increasing the load by a factor of 10% of Q_{cr} the delamination length decreases slightly, which means that no further delamination growth occurs; i.e. the delamination growth is arrested.

Fig. 7. Effect of elastic moduli on Q_{cr} .Fig. 8. Effect of elastic moduli on P_{cr} .Fig. 9. Effect of delamination on beam stiffness (at $Q = 22.2$ kN).

For an initial delamination length of 0.25 m the flat zone of the curve moves down, but the curve is still above the assumed G_{IC} value, which indicates an unstable delamination growth in the beam leading to a stable condition at the delamination length of around 0.48 m. However, in this case, Q_{cr} decreases by 60% to a value of 18.3 kN, when compared to the previous case for $L_d = 0.16$ m. For a further increase of delamination length to 0.38 m, the flat zone of the curve moves below the assumed G_{IC} value and, therefore, there is no delamination growth.

Compared to the initial case ($L_d = 0.16$ m), Q_{cr} in this case decreases by 80% to a value of 8.1 kN. From this observation, we may infer that delamination growth in a thin layer on the compression face of a beam is arrested, while in laminates under axial load the delamination growth can grow indefinitely. Additional experimental data are needed to corroborate this observation. Usually delamination buckling contributes to premature failure of glulam-GFRP beams reinforced on the compression face because the reinforcement ceases to be effective. After delamination, the wood laminate alone must carry any additional load. Test results of 5.79-m long beams, similar to the one

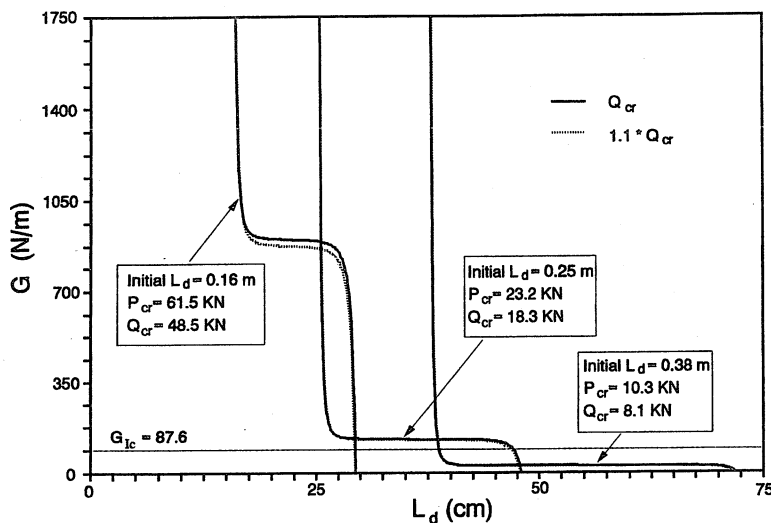


Fig. 10. Strain-energy release rate curves.

used in this example, indicated a significant decrease in the expected ultimate load due primarily to delamination of the top GFRP layer [7].

CONCLUSION

Most of the existing studies on delamination in laminated structures deal with an axial loading, irrespective of whether a thin-film model or a general bending model is used. However, the existing models can not be directly applied to a transverse load case in which the major concern is to find a critical transverse load. The main findings of this study are: (1) the internal axial force induced from a transverse load is close to Euler's column buckling load for a fixed-fixed boundary condition; (2) Euler's formula alone cannot be used to predict the critical transverse load (Q_{cr}); (3) an explicit form to relate the transverse load (Q) with the internal axial force (P) is established; (4) the critical load (Q_{cr}) can be accurately predicted as corroborated by experiment; and (5) a simulated delamination phenomenon indicates an unstable delamination growth after buckling of the delaminated sublaminates, followed by arrested delamination growth. This response is different to the axial loading case, for which unbounded delamination growth is generally predicted. To further verify the present model, it is desirable to conduct well-controlled tests of laminated beams with predetermined embedded delamination lengths and instrumented with transducers to

detect the onset of delamination buckling and measure delamination growth.

REFERENCES

- Chai, H., The growth of impact damage in compressively load laminates. Ph.D. dissertation, California Institute of Technology, Pasadena, CA, 1982.
- Yin, W.L., The effects of laminated structure on delamination buckling and growth. *J. Composite Mater.* 1958, **22**, (6), 502-517.
- Kardomateas, G.A. and Schmueser, D.W., Buckling and postbuckling of delaminated composites under compressive loads including transverse shear effects. *AIAA Jnl.* 1988, **26**, (3), 337-343.
- Chen, H.P., Shear deformation theory for compressive delamination buckling and growth. *AIAA Jnl.* 1991, **29**, (5), 813-819.
- Sheinman, I. and Soffer, M., Post-buckling analysis of composite delaminated beam. *Int. J. Solids Struct.* 1991, **27**, (5), 639-646.
- Tracy, J.J. and Pardoen, G.C., Effect of delamination on the flexural stiffness of composite laminates. *Thin-Walled Struct.* 1988, **6**, 371-383.
- Kim, Y., A layer-wise theory for linear and failure analysis of laminated composite beams. PhD dissertation, West Virginia University, Morgantown, WV, 1995.
- Reddy, J.N., Barbero, E.J. and Teply, J.L., A plate bending element based on a generalized laminate plate theory. *Int. J. Numer. Meth. Engng* 1989, **28**, 2275-2292.
- Barbero, E. J., On a generalized laminate theory with application to bending, vibration, and delamination buckling in composite laminates. Ph.D. dissertation, Virginia Polytechnic Institute and State University, Blacksburg, VA, 1989.
- Barbero, E.J. and Reddy, J.N., Modelling of delamination in composites laminates using a layer-wise plate theory. *Int. J. Solid Struct.* 1991, **28**, (3), 373-388.
- Lee, J., Gurdal, Z. and Griffin, O.H. Jr., Layer-wise approach for the bifurcation problem in laminated

- composites with delaminations. *AIAA Jnl.* 1993, **31**, (2), 331–338.
12. Sankar, B.V., A finite element for modeling delaminations in composite beams. *Comput. Struct.* 1991, **38**, (2), 239–246.
 13. Sankar, B.V. and Hu, S., Dynamic delamination propagation in composite beams. *J. Composite Mater.* 1991, **25**, (11), 1414–1426.
 14. Kutlu, Z. and Chang, F.K., Modeling compression failure of laminated composites containing multiple through-the-width delaminations. *J. Composite Mater.* 1992, **26**, (3), 350–387.
 15. Chen, W. F. and Lui, E. M., *Structural Stability*. Elsevier, New York, 1987.
 16. Barbero, E.J., Pultruded structural shapes—From the constituents to the structural behavior. *SAMPE Jnl.* 1991, **27**, (1), 25–30.
 17. Timoshenko, S. P. and Gere, J. M., *Theory of Elastic Stability*, 2nd edn. McGraw-Hill, New York, 1961.
 18. Ziegler, H., *Principles of Structural Stability*. Blaisdell Publishing, Massachusetts, 1968.

APPENDIX A

The total potential energy can be written as

$$\Pi = U_1 + U_2 + U_3 - Q\Delta \quad (\text{A1})$$

where Δ , the displacement at a loading point computed using eqn (8), is

$$\Delta = \frac{\theta(L-L_o)}{2} + \frac{Q(L-L_o)^2(L+2L_o-3L_d)}{24D_1} \quad (\text{A2})$$

The total potential energy along the post-buckling path can be expressed in terms of a single parameter (Q) as

$$\begin{aligned} \Pi = & \frac{1}{16} \frac{L_d[Q(L-L_o)-P_{cr}t]^2}{D_2} \\ & + \frac{1}{64} \frac{P_{cr}L_d^2[Q(L-L_o)-P_{cr}t]^2}{D_2^2[1-\cos(2\beta_{cr})]} \end{aligned}$$

$$\begin{aligned} & \left[L_d + \sin(2\beta_{cr}) \sqrt{\frac{D_3}{P_{cr}}} \right] \quad (\text{A3}) \\ & + \frac{P_{cr}^2 L_d}{4A_3} - \frac{QL_d(L-L_o)}{8D_2} [Q(L-L_o) - P_{cr}t] \\ & - \frac{Q^2(L-L_o)^2(L+2L_o-3L_d)}{48D_1} \end{aligned}$$

Then, the critical buckling load (bifurcation point) can be found as (see Timoshenko & Gere [17] and Ziegler [18], eqn (1.36), p. 11)

$$\frac{\sigma\pi}{\partial Q} = 0 \quad (\text{A4})$$

or

$$\begin{aligned} & \frac{3}{8} \frac{P_{cr}L_d^2[Q(L-L_o)-P_{cr}t]}{D_2^2 \sin^2 \beta_{cr}(L-L_o)} \\ & \times \left(L_d + \sqrt{\frac{D_3}{P_{cr}}} \sin 2\beta_{cr} \right) \\ & - \left(\frac{L+2L_o-3L_d}{D_1} + \frac{3L_d}{D_2} \right) Q = 0 \quad (\text{A5}) \end{aligned}$$

At the bifurcation point, the load Q in eqn (20) can be substituted into eqn (A5). Then, P_{cr} is found by an iterative numerical method using eqn (A5).